Two-photon resonant four-wave mixing in a dressed atomic system: Polarization interference in a Doppler-broadened system

Zhanchun Zuo,[1] Jiang Sun,[2] Xia Liu,[1] Ling-An Wu,[1] and Panming Fu[1]
[1]*Laboratory of Optical Physics, Beijing National Laboratory for Condensed Matter Physics, Institute of Physics, Chinese Academy of Sciences, Beijing 100080, China*
[2]*Department of Physics, Hebei University, Hebei, 071002, China*
(Received 5 September 2005; revised manuscript received 29 April 2006; published 2 February 2007)

We study dressed-atom two-photon resonant nondegenerate four-wave mixing (NFWM) in a Doppler-broadened system. It is found that there exists interference between the macroscopic field polarizations from different ensembles of atoms within the atomic velocity distribution. This polarization interference can cause significant modification of the NFWM spectra. We also show that two-photon resonant NFWM in dressed atoms can be employed as a new type of Doppler-free high-resolution Autler-Townes spectroscopy for measuring transition dipole moments between two highly excited atomic states.

DOI: 10.1103/PhysRevA.75.023805 PACS number(s): 42.65.−k, 42.50.Hz, 32.80.Rm

I. INTRODUCTION

Quantum interference has been a topic of interest for many years, and phenomena such as electromagnetically induced transparency (EIT) [1,2] have been predicted theoretically and demonstrated experimentally. By means of EIT, the linear and nonlinear optical properties of an atomic medium can be dramatically modified [3–5]. For example, Harris *et al.* [4] considered the efficiency of four-wave mixing (FWM) in a three-level system when a strong laser field induces EIT on a transition. They predicted an improvement in the conversion efficiency of many orders of magnitude, as compared to the weak-coupling field case. Petch *et al.* [6] showed that the efficiency of FWM can be increased even more when, in addition to a strong coupling field, the two-photon pump field also becomes strong. The exponential gain in resonant FWM has been investigated in a dressed-state analysis of a bichromatically driven three-level system [7]. On the other hand, the most impressive results obtained so far were seen in FWM in resonant Raman systems, which involved the generation of near-maximal coherence [8,9]. Quantum interference is also the basic phenomenon for controlling spontaneous emission [10].

Let us consider another type of interference, termed polarization interference. This involves interference between macroscopic field polarizations simultaneously excited in the medium and is quite different in physical origin from the quantum interference that is commonly referred to in the literature. Specifically, this phenomenon originates from an interference between transition amplitudes of indistinguishable quantum-mechanical pathways in an individual atom. By contrast, polarization interference involves interference between independent macroscopic polarizations, which are excited in the same or different types of atoms. More specifically, it is the interference of the radiation fields generated by these polarizations, so it is classic in nature. To distinguish between these two types of interferences, Koch *et al.* [11] considered transient FWM for two optical transitions, which are either coupled (e.g., in a three-level system) or uncoupled (e.g., in the case of two independent two-level absorbers). In the first case there exists quantum interference due to the coupling of the transitions via the common state, whereas in the latter case the polarization is a superposition of the individual temporal responses of the fields of the two-level systems, which interfere externally at the detector. Through detection of the time-resolved coherent signal they were able to distinguish between quantum and polarization beats without ambiguity.

Based on the polarization interference, various spectroscopic techniques have been developed. For example, Rothenberg and Grischkowsky [12] have observed a 1.9-psec polarization beat in sodium through impact excitation of both *D* lines by a 0.4-psec resonant laser pulse. DeBeer *et al.* [13] performed time-delayed FWM experiments in sodium vapor. Instead of using a single laser source, they used two laser beams of different frequencies to drive the $3S_{1/2}-3P_{1/2}$ and $3S_{1/2}-3P_{3/2}$ transitions, respectively. The FWM signal exhibits 1.9-psec modulation corresponding to the sodium *D*-line splitting when the time delay between two double-frequency pump beams increases. This technique has been extended by our group to the cascade three-level and four-level systems [14–17], based on nondegenerate four-wave mixing (NFWM) with a phase-conjugate geometry. For example, Fu *et al.* [15] demonstrated in Na vapor modulation of the NFWM signal intensity with a 55-fs period, corresponding to the beating between the resonant frequencies of the transitions from $3S_{1/2}$ to $3P_{3/2}$ and from $3P_{3/2}$ to $4D_{3/2,5/2}$. Mi *et al.* [16] observed signal modulation of period 25 fs, corresponding to the splitting between $5S$ and $4D$ of the Na. Polarization interference has also been successfully exploited to develop novel interferometric methods and to measure the parameters of various materials [18–20].

In Ref. [21] we studied two-photon resonant NFWM in a dressed-cascade four-level system. We found that in the presence of a strong coupling field, the two-photon resonant NFWM spectrum exhibits Autler-Townes (AT) splitting, accompanied by either suppression or enhancement of the NFWM signal. Such phenomena were demonstrated in Ba through inducing of atomic coherence between the ground state $6s^2$ and the doubly excited autoionizing Rydberg state $6pnd$. Although atomic coherence and quantum interference modify the properties of two-photon NFWM much like in EIT, there is a fundamental difference between conventional EIT-based FWM and the dressed-atom two-photon resonant

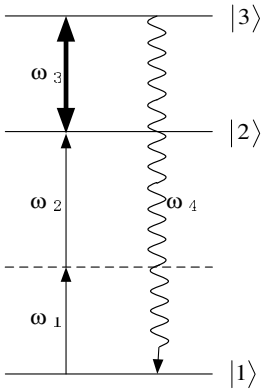

FIG. 1. Energy-level diagram for EIT-based FWM.

NFWM. Figure 1 presents a scheme of a typical EIT-based FWM, where one of the incident beams of the FWM process is a strong field at frequency ω_3 that induces transparency for the sum frequency $\omega_4=\omega_1+\omega_2+\omega_3$ on the $|3\rangle-|1\rangle$ resonance transition. By contrast, in the dressed-atom two-photon resonant NFWM a coupling field is applied to a transition which is not involved in the original NFWM process. We note that Tewari and Agarwal [22] have shown that the atomic dispersion and therefore the efficiency of the nonlinear generation at a given frequency can be controlled by the addition of an extra resonant laser field.

In this paper we shall study the dressed-atom two-photon resonant NFWM in Doppler-broadened systems. It is found that there exists interference between macroscopic polarizations from different ensembles of atoms within the atomic velocity distribution. This polarization interference is quite different from previous types. First, as mentioned before, most polarization interference originates from the interference between polarizations simultaneously excited in at least two distinct resonances, thus creating beats in the temporal behavior of the signal. By contrast, the interference discussed here involves the interference between polarizations induced in the same transition with a Doppler-shift frequency. Most importantly, we find that this polarization interference can be controlled by applying an additional coupling field.

We will also show in this paper that two-photon resonant NFWM in dressed atoms can be employed as a new type of Doppler-free high-resolution AT spectroscopy. As is well known, two bound states strongly coupled by an ac field manifest an energy splitting which is due to the oscillation of population between states in the presence of the driving field [23]. Numerous observations of this effect were reported for various wavelengths in gases [24,25], laser-cooled atoms [26], ions [27], and the solid state [28], in both steady-state and transient regimes [29,30]. Traditionally, an AT doublet is probed via a transition to a third level by detecting probe absorption, induced fluorescence, or photon ionization. The AT spectroscopy proposed here is different from previous types in that two-photon resonant NFWM is employed for probing the energy splitting. Since two-photon resonant NFWM can be employed in high-resolution laser spectroscopy [17], splittings which are much narrower than the Doppler linewidth can be measured. Moreover, our method involves a resonant three-photon transition; therefore, it can be employed for studying transitions between highly excited atomic states.

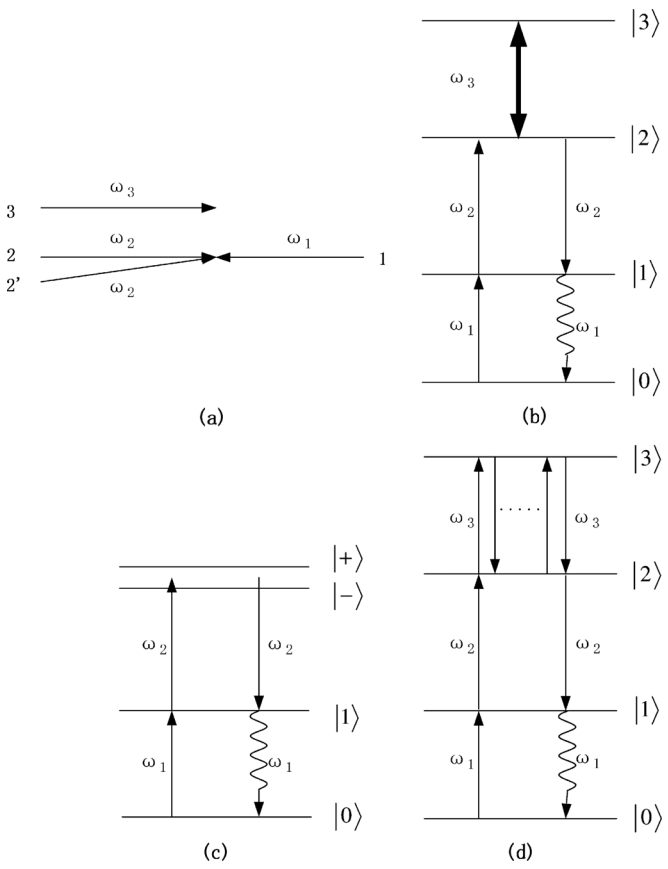

FIG. 2. (a) Schematic of dressed-atom two-photon resonant NFWM. (b) Energy-level diagram for dressed-atom two-photon resonant NFWM. (c) Dressed-state picture. (d) Schematic of $(2n+4)$-wave mixing.

II. BASIC THEORY

Let us consider a cascade four-level system [Fig. 2(b)], where states between $|0\rangle$ and $|1\rangle$, between $|1\rangle$ and $|2\rangle$, and between $|2\rangle$ and $|3\rangle$ are coupled by dipolar transitions with resonant frequencies Ω_1, Ω_2, and Ω_3 and dipole moment matrix elements μ_1, μ_2, and μ_3, respectively. We first consider two-photon resonant NFWM in the $|0\rangle$-$|1\rangle$-$|2\rangle$ cascade three-level system. As shown in Fig. 2(a), beams 2 and 2′ have the same frequency ω_2 and a small angle exists between them; beam 1 with frequency ω_1 propagates along the opposite direction of beam 2. We assume that $\omega_1 \simeq \Omega_1$ and $\omega_2 \simeq \Omega_2$, so that ω_1 drives the transition from $|0\rangle$ to $|1\rangle$ while ω_2 drives the transition from $|1\rangle$ to $|2\rangle$. In this case, the simultaneous interactions of atoms with beams 1 and 2 will induce atomic coherence between $|0\rangle$ and $|2\rangle$ through two-photon excitation. This coherence is then probed by beam 2′, and as a result an NFWM signal of frequency ω_1, which propagates almost opposite to beam 2′, is generated. Now, we apply a coupling laser (beam 3) of frequency ω_3 $(\simeq\Omega_3)$, which propagates along the direction of beam 2, to drive the transition from $|2\rangle$ to $|3\rangle$. In the bare-state picture, atomic

coherence is induced between states $|0\rangle$ and $|3\rangle$. On the other hand, in the dressed-state picture [Fig. 2(c)], the coupling field creates dressed atomic states $|+\rangle$ and $|-\rangle$, which are the superpositions of the states $|2\rangle$ and $|3\rangle$.

Let the Δ's represent various detunings: $\Delta_1=\Omega_1-\omega_1$, $\Delta_2=\Omega_2-\omega_2$, and $\Delta_3=\Omega_3-\omega_3$. After a canonical transformation the effective Hamiltonian is

$$H=\hbar\,\Delta_1|1\rangle\langle 1|+\hbar\,(\Delta_1+\Delta_2)|2\rangle\langle 2|+\hbar\,(\Delta_1+\Delta_2+\Delta_3)|3\rangle\langle 3| - (\mu_1 E_1|1\rangle\langle 0|+\mu_2 E_2|2\rangle\langle 1|+\mu_3 E_3|3\rangle\langle 2|+\mathrm{H.c}). \quad (1)$$

Here, $E_1=\varepsilon_1 e^{i\mathbf{k}_1\cdot\mathbf{r}}$, $E_2=\varepsilon_2 e^{i\mathbf{k}_2\cdot\mathbf{r}}+\varepsilon_2' e^{i\mathbf{k}_2'\cdot\mathbf{r}}$, and $E_3=\varepsilon_3 e^{i\mathbf{k}_3\cdot\mathbf{r}}$ are the complex incident laser fields with frequencies ω_1, ω_2, and ω_3, respectively; while $\mathbf{k}_1$, $\mathbf{k}_2$, $\mathbf{k}_2'$, and $\mathbf{k}_3$ are the wave vectors of beams 1, 2, 2′, and 3, respectively. The nonlinear polarization responsible for the two-photon resonant NFWM signal is proportional to the off-diagonal density matrix element ρ_{10}. We will assume, as usual, that ε_1, ε_2, and ε_2' are weak, whereas the coupling field ε_3 can be of arbitrary magnitude. Thus ρ_{10} needs to be calculated to the order $\varepsilon_1\varepsilon_2\varepsilon_2'$, but to all orders in ε_3. This can be done using density matrix equations with relaxation terms properly included:

$$\frac{d\rho}{dt}=-\frac{i}{\hbar}[H,\rho]+\left(\frac{d\rho}{dt}\right)_{relax}. \quad (2)$$

We obtain [21]

$$\rho_{10}(\mathbf{r})=-i\frac{G_1 G_2 (G_2')^*[i(\Delta_1+\Delta_2+\Delta_3)+\Gamma_{30}]\exp[i(\mathbf{k}_1+\mathbf{k}_2-\mathbf{k}_2')\cdot\mathbf{r}]}{(i\Delta_1+\Gamma_{10})^2\{[i(\Delta_1+\Delta_2)+\Gamma_{20}][i(\Delta_1+\Delta_2+\Delta_3)+\Gamma_{30}]+|G_3|^2\}}, \quad (3)$$

where Γ_{n0} is the transverse relaxation rate between states $|n\rangle$ and $|0\rangle$; the G's denote the coupling coefficients $G_1=\mu_1\varepsilon_1/\hbar$, $G_2=\mu_2\varepsilon_2/\hbar$, $G_2'=\mu_2\varepsilon_2'/\hbar$, and $G_3=\mu_3\varepsilon_3/\hbar$. According to Eq. (3), the NFWM signal propagates along the direction $\mathbf{k}_p=\mathbf{k}_1+\mathbf{k}_2-\mathbf{k}_2'$.

A. Dressed-atom two-photon resonant NFWM in a Doppler-broadened system

Let us consider the Doppler effect. The nonlinear polarization $P^{NL}(\mathbf{r})$ responsible for the NFWM signal is given by averaging over the velocity distribution function $W(\mathbf{v})$—i.e.,

$$P^{NL}(\mathbf{r})=N\mu_1\int_{-\infty}^{\infty}d\mathbf{v}W(\mathbf{v})\rho_{10}(\mathbf{r},\mathbf{v}). \quad (4)$$

Here $\rho_{10}(\mathbf{r},\mathbf{v})$ is obtained from Eq. (3) by using the Doppler-shift frequencies and N is the density of the atoms, while

$$W(\mathbf{v})=\frac{1}{\sqrt{\pi}u}\exp[-(v/u)^2], \quad (5)$$

where $u=\sqrt{2KT/m}$, with m being the mass of an atom, K is Boltzmann's constant, and T the absolute temperature. In a typical NFWM experiment, the intersection angle between beams 2 and 2′ is small; therefore, it is permissible to set $\mathbf{k}_1=-k_1\mathbf{z}$, $\mathbf{k}_2=k_2\mathbf{z}$, $\mathbf{k}_2'\simeq k_2\mathbf{z}$, and $\mathbf{k}_3=k_3\mathbf{z}$. We obtain finally

$$P^{NL}(\mathbf{r})=P_T\exp(i\mathbf{k}_p\cdot\mathbf{r}), \quad (6)$$

with

$$P_T\simeq -i\frac{\hbar N}{\sqrt{\pi}u}\left(\frac{\mu_1}{\hbar}\right)^2\left(\frac{\mu_2}{\hbar}\right)^2\varepsilon_1\varepsilon_2(\varepsilon_2')^* \times\exp(-i\omega_1 t)\int_{-\infty}^{\infty}dv e^{-(v/u)^2}F(v). \quad (7)$$

Here

$$F(v)=\frac{i[\Delta_1+\Delta_2+\Delta_3-k_1(1-\zeta_2-\zeta_3)v]+\Gamma_{30}}{\{i[\Delta_1+\Delta_2-k_1(1-\zeta_2)v]+\Gamma_{20}\}\{i[\Delta_1+\Delta_2+\Delta_3-k_1(1-\zeta_2-\zeta_3)v]+\Gamma_{30}\}+|G_3|^2}\times\frac{1}{[i(\Delta_1-k_1v)+\Gamma_{10}]^2}, \quad (8)$$

with $\zeta_2=k_2/k_1$ and $\zeta_3=k_3/k_1$. Physically, $F(v)$ is proportional to the nonlinear polarization $P(v)$ of atoms with velocity v. On the other hand, the signal intensity is proportional to $|P_T|^2$.

B. Interfering paths

The form of ρ_{10} [Eq. (3)] that we obtain from solving the equation of motion of the density matrix elements in the steady state is not intuitive at first glance. If we express ρ_{10} as a power expansion in the coupling coefficient G_3 in a perturbative approach, then each term corresponds to a definite wave-mixing process. Although a calculation involving only low-order processes would not be satisfactory in the limit of large G_3, this figure does show how the amplitudes of different order processes can interfere to cause suppression or enhancement of the NFWM signal.

We rewrite Eq. (3) in the form

$$\rho_{10}(\mathbf{r}) = -i\frac{G_1 G_2 (G_2')^* \exp[i(\mathbf{k}_1+\mathbf{k}_2-\mathbf{k}_2')]}{(i\Delta_1+\Gamma_{10})^2[i(\Delta_1+\Delta_2)+\Gamma_{20}]}\left(1+\frac{|G_3|^2}{[i(\Delta_1+\Delta_2)+\Gamma_{20}][i(\Delta_1+\Delta_2+\Delta_3)+\Gamma_{30}]}\right)^{-1}. \tag{9}$$

If $|G_3|^2/\Gamma_{20}\Gamma_{30}<1$, then through power expansion, we obtain

$$\rho_{10}(\mathbf{r}) = -i\frac{G_1 G_2 (G_2')^* \exp[i(\mathbf{k}_1+\mathbf{k}_2-\mathbf{k}_2')]}{(i\Delta_1+\Gamma_{10})^2[i(\Delta_1+\Delta_2)+\Gamma_{20}]}\left(1-\frac{|G_3|^2}{[i(\Delta_1+\Delta_2)+\Gamma_{20}][i(\Delta_1+\Delta_2+\Delta_3)+\Gamma_{30}]}+\cdots\right.$$
$$\left.+(-1)^n\frac{|G_3|^{2n}}{[i(\Delta_1+\Delta_2)+\Gamma_{20}]^n[i(\Delta_1+\Delta_2+\Delta_3)+\Gamma_{30}]^n}\right). \tag{10}$$

It can be proved easily that the term containing $|G_3|^{2n}$ in Eq. (10) corresponds to a $(2n+4)$-wave mixing process described by the perturbation chain: $\rho_{00}^{(0)}\rightarrow\rho_{10}^{(1)}\rightarrow\rho_{20}^{(2)}\rightarrow\rho_{30}^{(3)}\rightarrow\rho_{20}^{(4)}\rightarrow\cdots\rightarrow\rho_{30}^{(2n+1)}\rightarrow\rho_{20}^{(2n+2)}\rightarrow\rho_{10}^{(2n+3)}$, as shown in Fig. 2(d).

Let us consider the weak-coupling-field limit. In this case, the dressed-atom two-photon resonant NFWM can be regarded as heterodyne detection of the six-wave mixing with the four-wave mixing signal as the optical local oscillator. If we retain only the first and second terms, then Eq. (10) can be rewritten as

$$\rho_{10}\propto L-\frac{|G_3|^2}{i(\Delta_1+\Delta_2+\Delta_3)+\Gamma_{30}}, \tag{11}$$

where $L=i(\Delta_1+\Delta_2)+\Gamma_{20}$. The line shape of the NFWM spectrum is sensitive to the phase of L. When $\Delta_1+\Delta_2=0$, L is real and the NFWM spectrum manifests the real part of the second term in Eq. (11), which exhibits an absorption line shape—i.e., suppression of the NFWM signal. By contrast, L becomes imaginary for large frequency detuning (i.e., $|\Delta_1+\Delta_2|\gg\Gamma_{30}$). In this case, the imaginary part of $|G_3|^2/[i(\Delta_1+\Delta_2+\Delta_3)+\Gamma_{30}]$ is explored, leading to the dispersion line shape in the NFWM spectrum.

III. POLARIZATION INTERFERENCE

A. Polarization interference in two-photon resonant NFWM

Let us first consider the polarization interference in two-photon resonant NFWM. As is well known, the NFWM signal is a coherent beam; therefore, in a Doppler-broadened system there exists interference between radiation generated by polarizations of atoms that have different velocities. This polarization interference can have a strong impact on the NFWM spectrum. Figure 3 presents the NFWM spectra for $\Delta_1/\Gamma_{20}=0$ and $\Gamma_{10}/k_1u=\Gamma_{20}/k_1u=0.02$, with values of $\zeta_2=0.6$ (solid curve), 0.8 (dashed curve), 1 (dotted curve), and 1.2 (dot-dashed curve). We can see that the linewidths of the spectra equal approximately the homogeneous linewidth $2\Gamma_{20}$ of the system when $\zeta_2\geq 1$. However, the linewidth becomes much broader when $\zeta_2<1$. Correspondingly, the signal intensities also decrease drastically. To investigate how the interference between macroscopic polarizations from different ensembles of atoms affects the NFWM spectrum, instead of calculating $|\int_{-\infty}^{\infty}dve^{-(v/u)^2}P(v)|^2$, we sum up the signal intensities of individual atoms—i.e., $\int_{-\infty}^{\infty}dve^{-(v/u)^2}|P(v)|^2$ (thin solid curve in Fig. 3). For the former case, there exists polarization interference of atoms with different velocities, while the polarization interference is neglected for the latter case. It is found that the line shape is narrow and basically independent of the values of ζ_2 when the polarization interference is neglected. This indicates that the broadening of the NFWM spectra linewidths for $\zeta_2<1$ is due to the polarization interference.

The role of polarization interference in two-photon resonant NFWM can be clarified further by studying the real and imaginary parts of $F(v)$, which is proportional to the polarization $P(v)$ of atoms with velocity v. Figures 4(a) and 4(b) present the real part $F'(v)$ (solid curves), imaginary part $F''(v)$ (dashed curves), and absolute value $|F(v)|$ (dotted curves) of $F(v)$ for $\zeta_2=0.8$ and 1.2, respectively, when $\Delta_1/\Gamma_{20}=\Delta_2/\Gamma_{20}=0$ and $\Gamma_{10}/k_1u=\Gamma_{20}/k_1u=0.02$. In the first place, since $\Delta_1/\Gamma_{10}=0$, only atoms with velocity $|v|\lesssim\Gamma_{10}/k_1$ can be resonantly excited by beam 1 and so contribute to the NFWM signal. Second, the imaginary part $F''(v)$ shows a dispersive line shape, which leads to

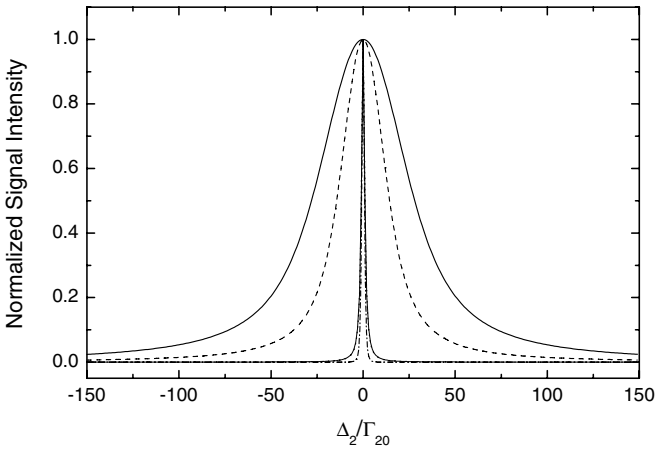

FIG. 3. NFWM spectra for $\Delta_1/\Gamma_{20}=0$, $\Gamma_{10}/k_1u=\Gamma_{20}/k_1u=0.02$, and values of $\zeta_2=0.6$ (solid curve), 0.8 (dashed curve), 1 (dotted curve), and 1.2 (dot-dashed curve). The thin solid curve presents the corresponding result when polarization interference is neglected.

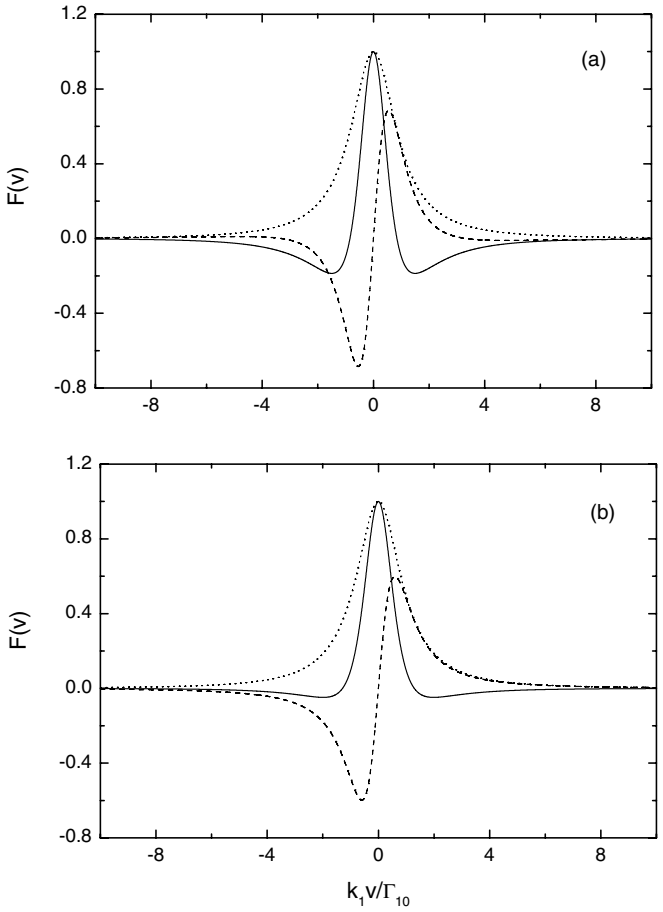

FIG. 4. Real part $F'(v)$ (solid curves), imaginary part $F''(v)$ (dashed curves), and absolute value $|F(v)|$ (dotted curves) of $F(v)$ for (a) $\zeta_2 = 0.8$ and (b) $\zeta_2 = 1.2$.

$\int_{-\infty}^{\infty} dv e^{-(v/u)^2} F''(v) = 0$; therefore, only the real part $F'(v)$ contributes to the signal. Finally, since $F'(v)$ changes sign on the wings of both the $v<0$ and $v>0$ sides, destructive polarization interference occurs between atoms, thereby suppressing the total polarization P_T. The degree of destructive interference depends on ζ_2. Figure 5 presents $|P_T|$ versus ζ_2 for $\Delta_1/\Gamma_{20}=0$ and $\Gamma_{10}/k_1u=\Gamma_{20}/k_1u=0.02$, with Δ_2/Γ_{20} given above the curves. We take the spectrum at $\zeta_2 = 1.2$, where the linewidth is narrow, as reference by normalizing $|P_T|$ to 1 at $\zeta_2 = 1.2$. We see that $|P_T|$ with $\Delta_2/\Gamma_{20}<1$ is reduced significantly compared to that with $\Delta_2/\Gamma_{20}>1$ when $\zeta_2<1$. Since interference mainly suppresses the center of the line when $\zeta_2<1$, it causes broadening of the NFWM spectrum.

B. Controlling polarization interference by applying an additional coupling field

The degree of destructive interference can be controlled by applying a weak coupling field (beam 3) of frequency ω_3 to drive the transition between $|2\rangle$ and $|3\rangle$ [see Fig. 2(b)]. Figure 6 presents the NFWM spectra with coupling coefficient $G_3/\Gamma_{30} = 0$ (dot-dashed curve), 0.05 (dotted curve), 0.15 (dashed curve), and 0.2 (solid curve) when the coupling field is exactly on resonance (i.e., $\Delta_3/\Gamma_{30}=0$). Other parameters are $\zeta_2=0.8$, $\zeta_3=1.2$, $\Delta_1/\Gamma_{20}=0$, and $\Gamma_{10}/k_1u=\Gamma_{20}/k_1u=\Gamma_{30}/k_1u=0.02$. In general, the spectra consist of a narrow line and a broad background in the presence of the coupling field. The broad background decreases as the coupling coefficient increases. More specifically, when the coupling field is very weak, a narrow dip appears first at the center of the line (dotted curve). The line shape of the spectrum then converts to a single line of homogeneous linewidth with the broad background completely suppressed when $G_3/\Gamma_{30} = 0.2$ (solid curve). For further increase of the coupling field strength, the NFWM spectrum will exhibit an AT doublet, as will be discussed in the next section.

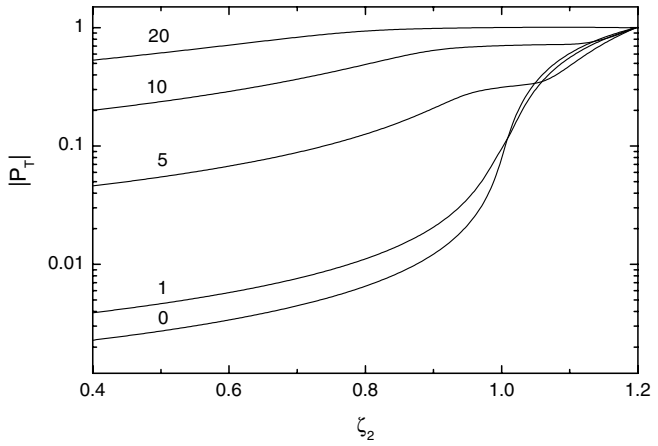

FIG. 5. $|P_T|$ versus ζ_2 for $\Delta_1/\Gamma_{20}=0$ and $\Gamma_{10}/k_1u=\Gamma_{20}/k_1u=0.02$ with Δ_2/Γ_{20} given above the curves in the figure. We normalize $|P_T|$ to 1 at $\zeta_2 = 1.2$.

C. Suppression and enhancement of the NFWM signal

Let us now investigate the NFWM spectrum when we scan Δ_3 while keeping Δ_1 and Δ_2 fixed. Figure 7 presents the Δ_3 dependence of the NFWM signal intensity at exact one-

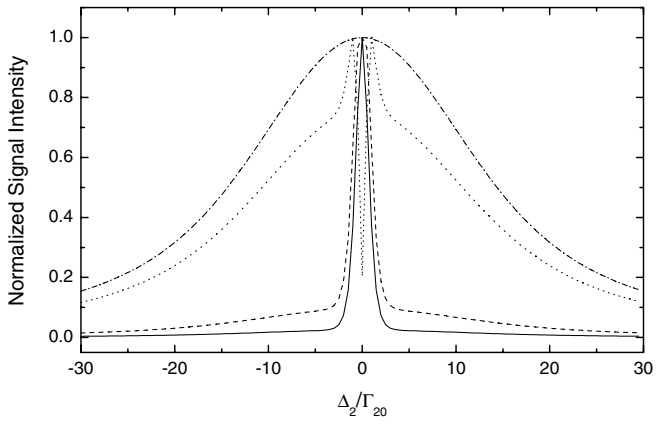

FIG. 6. NFWM spectra with coupling coefficient $G_3/\Gamma_{30} = 0$ (dot-dashed curve), 0.05 (dotted curve), 0.15 (dashed curve), and 0.2 (solid curve) when the coupling field is exactly on resonance (i.e., $\Delta_3/\Gamma_{30}=0$). Other parameters are $\zeta_2=0.8$, $\zeta_3 =1.2$, $\Delta_1/\Gamma_{20}=0$, and $\Gamma_{10}/k_1u=\Gamma_{20}/k_1u=\Gamma_{30}/k_1u=0.02$.

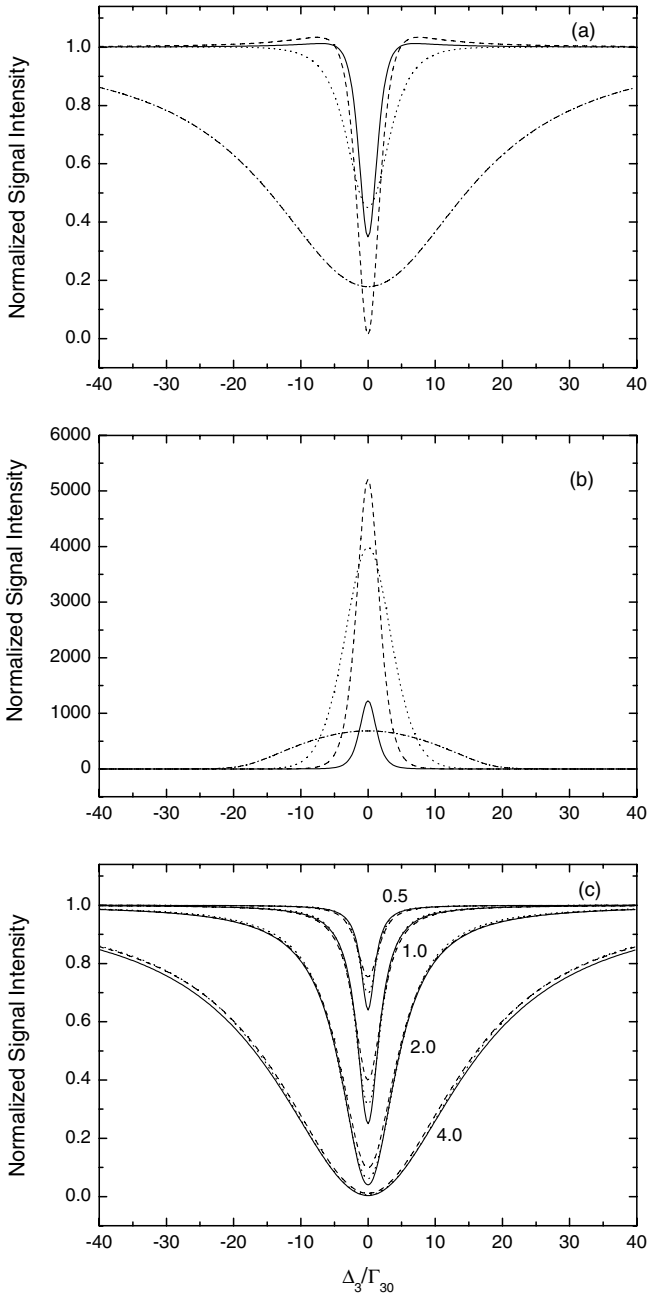

FIG. 7. NFWM signal intensity versus detuning Δ_3 at exact one-photon and two-photon resonance (i.e., $\Delta_1/\Gamma_{10}=0$ and $\Delta_2/\Gamma_{20}=0$) for (a) $\zeta_2=1.2$ and $\zeta_3=1.2$ and (b) $\zeta_2=0.8$ and $\zeta_3=1.2$ when $\Gamma_{10}/k_1u=\Gamma_{20}/k_1u=\Gamma_{30}/k_1u=0.02$ and $G_3/\Gamma_{30}=0.5$ (solid curve), 1 (dashed curve), 2 (dotted curve), and 4 (dot-dashed curve). On the other hand, (c) presents the corresponding results (G_3/Γ_{30} is given near the curves) when polarization interference is neglected with $\zeta_2=1.2$ (dashed curves), $\zeta_2=0.8$ (dotted curves), and the homogeneously broadened cases (solid curves). The NFWM signal intensity with no coupling field is normalized to 1.

photon and two-photon resonance (i.e., $\Delta_1/\Gamma_{10}=0$ and $\Delta_2/\Gamma_{20}=0$) for (a) $\zeta_2=1.2$ and $\zeta_3=1.2$ and (b) $\zeta_2=0.8$ and $\zeta_3=1.2$, when $\Gamma_{10}/k_1u=\Gamma_{20}/k_1u=\Gamma_{30}/k_1u=0.02$, and $G_3/\Gamma_{30}=0.5$ (solid curve), 1 (dashed curve), 2 (dotted curve), and 4 (dot-dashed curve). For comparison, the solid curves in Fig. 7(c) present the corresponding results (G_3/Γ_{30} is given near

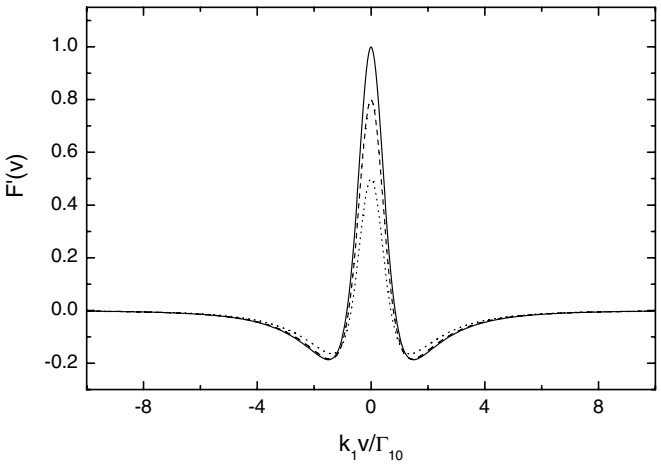

FIG. 8. $F'(v)$ for $G_3/\Gamma_{30}=0$ (solid curve), 0.5 (dashed curve), and 1 (dotted curve) when the coupling field is exactly on resonance (i.e., $\Delta_3/\Gamma_{30}=0$). Other parameters are $\Delta_1/\Gamma_{10}=\Delta_2/\Gamma_{20}=0$, $\zeta_2=0.8$, $\zeta_3=1.2$, and $\Gamma_{10}/k_1u=\Gamma_{20}/k_1u=\Gamma_{30}/k_1u=0.02$.

the curves) for the homogeneously broadened case. In these figures the NFWM signal intensity with no coupling field is normalized to 1. Let us first consider the case when $\zeta_2=1.2$ [Fig. 7(a)]. We see that the NFWM signal intensity is suppressed when the frequency of the coupling field is scanned across the resonance. The depth of the dip increases first as G_3/Γ_{30} increases, then decreases while the linewidth of the dip becomes broader. A further increase of G_3/Γ_{30} causes an increase of both the depth and the linewidth of the dip. This is different from the homogeneously broadened cases [solid curves in Fig. 7(c)], which show a monotonic increase of both the depth and the linewidth as G_3/Γ_{30} increases. From the dressed-model viewpoint [Fig. 2(c)], suppression of the NFWM is due to the splitting induced by the coupling field, leading to detuning of the two-photon resonance. To study the anomalous behavior in the Doppler-broadened system, we neglect polarization interference and calculate $\int_{-\infty}^{\infty}dv\ e^{-(v/u)^2}|P(v)|^2$; the results are shown in Fig. 7(c) (dashed curves), which are consistent with those of the homogeneously broadened case, proving that the anomalous behavior in the Doppler-broadened system is due to the polarization interference.

The Δ_3 dependence of the NFWM signal intensity for $\zeta_2<1$ is in sharp contrast with that of $\zeta_2>1$. As shown in Fig. 7(b), application of the coupling field causes enhancement of the NFWM signal intensity. Specifically, as G_3/Γ_{30} increases, the NFWM signal intensity first increases, then decreases with broader linewidths. The dotted curves in Fig. 7(c) are the corresponding results when polarization interference is neglected, again showing that the enhancement of the NFWM signal is due to the polarization interference. This can be understood through studying the influence of the coupling field on $F'(v)$. Figure 8 presents $F'(v)$ for $G_3/\Gamma_{30}=0$ (solid curve), 0.5 (dashed curve), and 1 (dotted curve) when the coupling field is exactly on resonance. We can see that, when $G_3/\Gamma_{30}=0$, the interference between the nonlinear polarizations of atoms with different velocities causes a significant reduction of the NFWM signal intensity. However,

application of the coupling field suppresses mainly the polarizations of atoms with $v=0$, leading to a reduction of the degree of destructive interference. As a result, the NFWM signal intensity is enhanced.

We next investigate the spectrum for a weak coupling field when $\Delta_2/\Gamma_{20}\neq 0$. Figure 9 presents the Δ_3 dependence of the NFWM signal intensity when $G_3/\Gamma_{30}=0.5$, $\zeta_3=1.2$, $\Gamma_{10}/k_1u=\Gamma_{20}/k_1u=\Gamma_{30}/k_1u=0.02$, and $\Delta_1/\Gamma_{10}=0$, for values of (a) $\zeta_2=1.2$ and (b) $\zeta_2=1$ and $\Delta_2/\Gamma_{20}=0$ (solid curve), -1 (dashed curve), -4 (dotted curve), and -10 (dot-dashed curve). On the other hand, Fig. 9(c) presents the corresponding results (Δ_2/Γ_{20} is given near the curves) when polarization interference is neglected, with $\zeta_2=1.2$ (dashed curves), $\zeta_2=1$ (dotted curves), and the homogeneously broadened cases (solid curves). Here, the NFWM signal intensity with no coupling field is normalized to 1. First, the spectra of the homogeneously broadened case change from an absorption to a dispersion line shape as Δ_2/Γ_{20} varies from 0 to -10. This phenomenon is due to the interference between four-wave and six-wave mixing, as pointed out in Sec. II B. On the other hand, due to the polarization interference, the spectra of $\zeta_2=1.2$ [Fig. 9(a)] exhibit deeper dips, while the spectra of $\zeta_2=1$ [Fig. 9(b)] change from a peak to a dispersion line shape as Δ_2/Γ_{20} varies from 0 to -10.

Finally, let us consider the Δ_3 dependence of the spectrum for a strong coupling field and large two-photon detuning. In this case, the coupling field drives the transition between $|2\rangle$ and $|3\rangle$ and creates dressed states $|+\rangle$ and $|-\rangle$ [see Fig. 2(c)]. Therefore, although the NFWM signal for large two-photon detuning is extremely small when $G_3=0$, the strong coupling field can cause resonant excitation of one of the dressed states. The resonant condition is given by $\Delta_3=[|G_3|^2-(\Delta_1+\Delta_2)^2]/(\Delta_1+\Delta_2)$ [21]. In Fig. 10(a) we present the Δ_3 dependence of the NFWM signal intensity for $\zeta_2=1.2$ (solid curves) and $\zeta_2=0.8$ (dashed curves) when $G_3/\Gamma_{30}=50$, $\zeta_3=1.2$, $\Gamma_{10}/k_1u=\Gamma_{20}/k_1u=\Gamma_{30}/k_1u=0.02$, and $\Delta_1/\Gamma_{10}=0$. The values of Δ_2/Γ_{20} are written close to the curves. On the other hand, Fig. 10(b) presents the corresponding results when polarization interference is neglected, for $\zeta_2=1.2$ (solid curves), $\zeta_2=0.8$ (dashed curves), and the homogeneously broadened cases (dotted curves). Comparing the Doppler-broadened and homogeneously broadened cases, the most profound effect of polarization interference is that it significantly increases the resonant enhancement. For example, when $\Delta_2/\Gamma_{30}=-70$ the NFWM signal is enhanced by a factor of 2.9×10^5 for the Doppler-broadened system with $\zeta_2=1.2$, instead of 5.6×10^2 for the homogeneously broadened system. The huge enhancement of the signal in the former is due to the fact that the strong coupling field can not only induce resonance enhancement but can also suppress the destructive polarization interference.

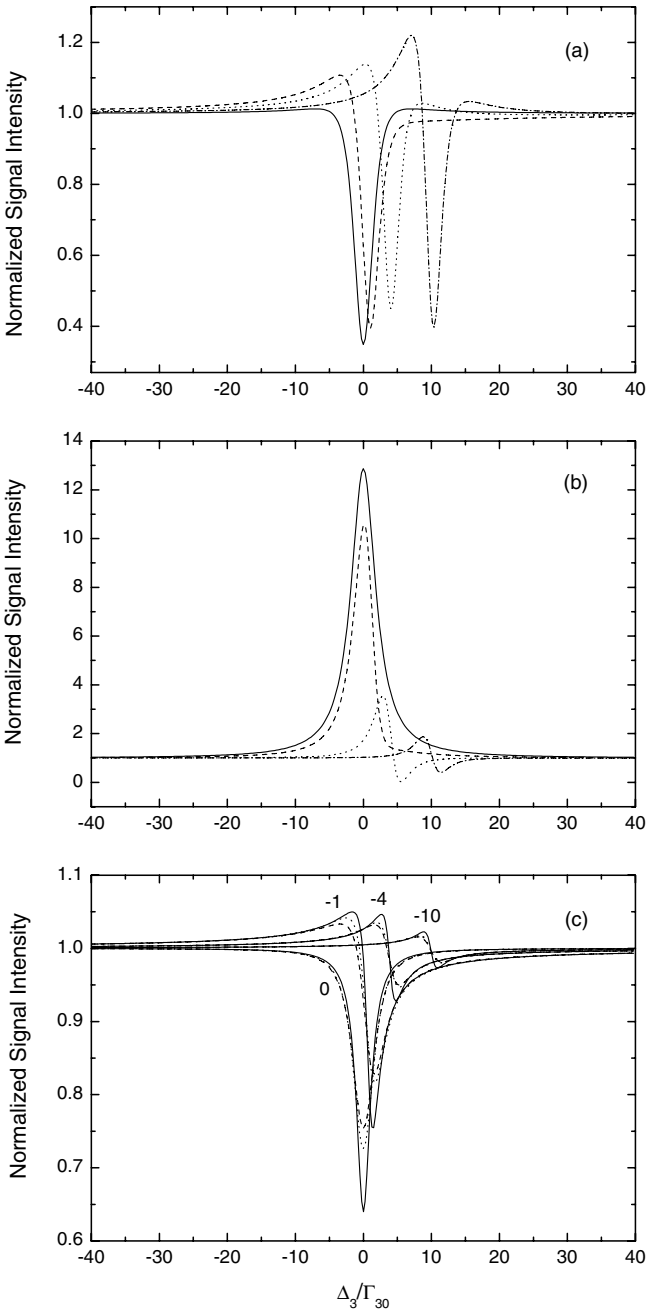

FIG. 9. NFWM signal intensity versus detuning Δ_3 for (a) $\zeta_2=1.2$ and (b) $\zeta_2=1$ when $G_3/\Gamma_{30}=0.5$, $\zeta_3=1.2$, $\Gamma_{10}/k_1u=\Gamma_{20}/k_1u=\Gamma_{30}/k_1u=0.02$, and $\Delta_1/\Gamma_{10}=0$, for values of $\Delta_2/\Gamma_{20}=0$ (solid curve), -1 (dashed curve), -4 (dotted curve), and -10 (dot-dashed curve). On the other hand, (c) presents the corresponding results (Δ_2/Γ_{20} is given near the curves) when polarization interference is neglected with $\zeta_2=1.2$ (dashed curves), $\zeta_2=1$ (dotted curves), and the homogeneously broadened cases (solid curves). Here the NFWM signal intensity with no coupling field is normalized to 1.

IV. AUTLER-TOWNES SPLITTING

As is well known, an AT doublet is due to the oscillation of population between states in the presence of a driving field. In Ref. [21] we have shown that, in a homogeneously broadened system, two-photon resonant NFWM can be employed for probing the energy splitting. In this section we will discuss how the Doppler effect affects the AT spectrum.

We consider the case when ω_1 is within the Doppler profile of the transition from $|0\rangle$ to $|1\rangle$. Figure 11 presents the NFWM spectra in the presence of the coupling field for $G_3/\Gamma_{30}=0$ (solid curve), 1 (dashed curve), 10 (dotted

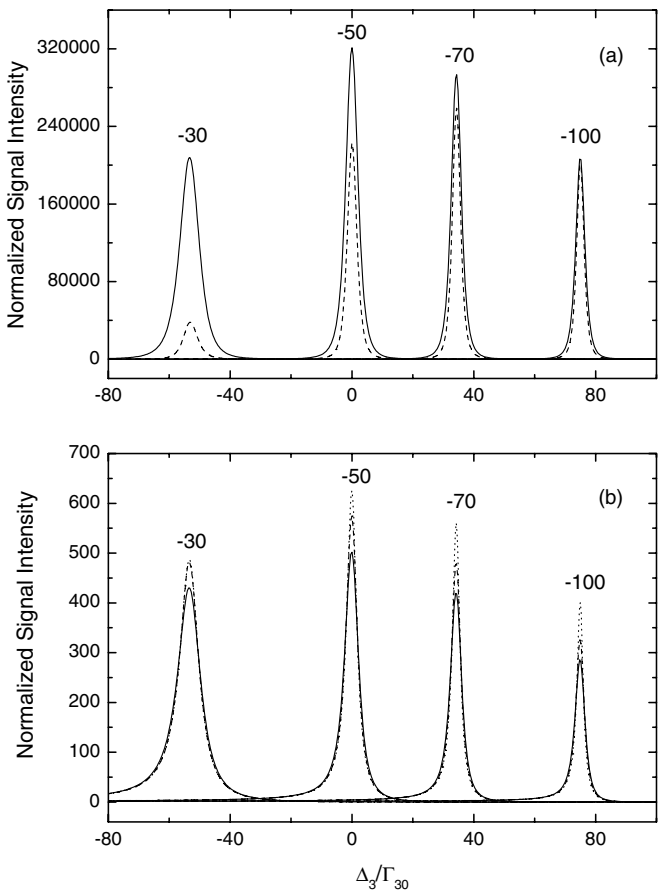

FIG. 10. (a) NFWM signal intensity versus detuning Δ_3 for $\zeta_2=1.2$ (solid curves) and $\zeta_2=0.8$ (dashed curves) when $G_3/\Gamma_{30}=50$, $\zeta_3=1.2$, $\Gamma_{10}/k_1u=\Gamma_{20}/k_1u=\Gamma_{30}/k_1u=0.02$, and $\Delta_1/\Gamma_{10}=0$. The values of Δ_2/Γ_{20} are shown above the peaks. On the other hand, (b) presents the corresponding results when polarization interference is neglected with $\zeta_2=1.2$ (solid curves), $\zeta_2=0.8$ (dashed curves), and the homogeneously broadened cases (dotted curves). Here, the NFWM signal intensity with no coupling field is normalized to 1.

curve), and 20 (dot-dashed curve) when both ω_1 and ω_3 are exactly on resonance (i.e., $\Delta_1/\Gamma_{30}=\Delta_3/\Gamma_{30}=0$). Other parameters are $\Gamma_{10}/k_1u=\Gamma_{20}/k_1u=\Gamma_{30}/k_1u=0.02$, $\zeta_3=1.2$, and ζ_2 = (a) 1.2 and (b) 0.8. For comparison, Fig. 11(c) presents the corresponding curves of the homogeneously broadened cases. In general, the AT spectrum is Doppler free. On the other hand, as discussed in the previous section, due to the polarization interference, the linewidth of the NFWM spectrum is much larger than the homogeneous linewith in the absence of the coupling field when $\zeta_2=0.8$ [solid curve in Fig. 11(b)]. As G_3/Γ_{30} increases, the linewidth first becomes narrower, then exhibits Doppler-free AT splitting again. This Doppler-free characteristic of the AT spectrum is due to the fact that only the atoms which have velocity $v\simeq\Delta_1/k_1$ along the **z** axis are resonant with beam 1 and so can contribute to the signal (see Fig. 4). Figure 12 presents the G_3 dependence of the AT splitting Δ_{AT} for $\zeta_2=1.2$ (solid curve) and 0.8 (dashed curve) with all the other parameters the same as those used in Fig. 11. Similar to the homogeneously broadened cases [21] we have $\Delta_{AT}\simeq 2G_3$ in the limit of $G_3\gg\Gamma_{20},\Gamma_{30}$.

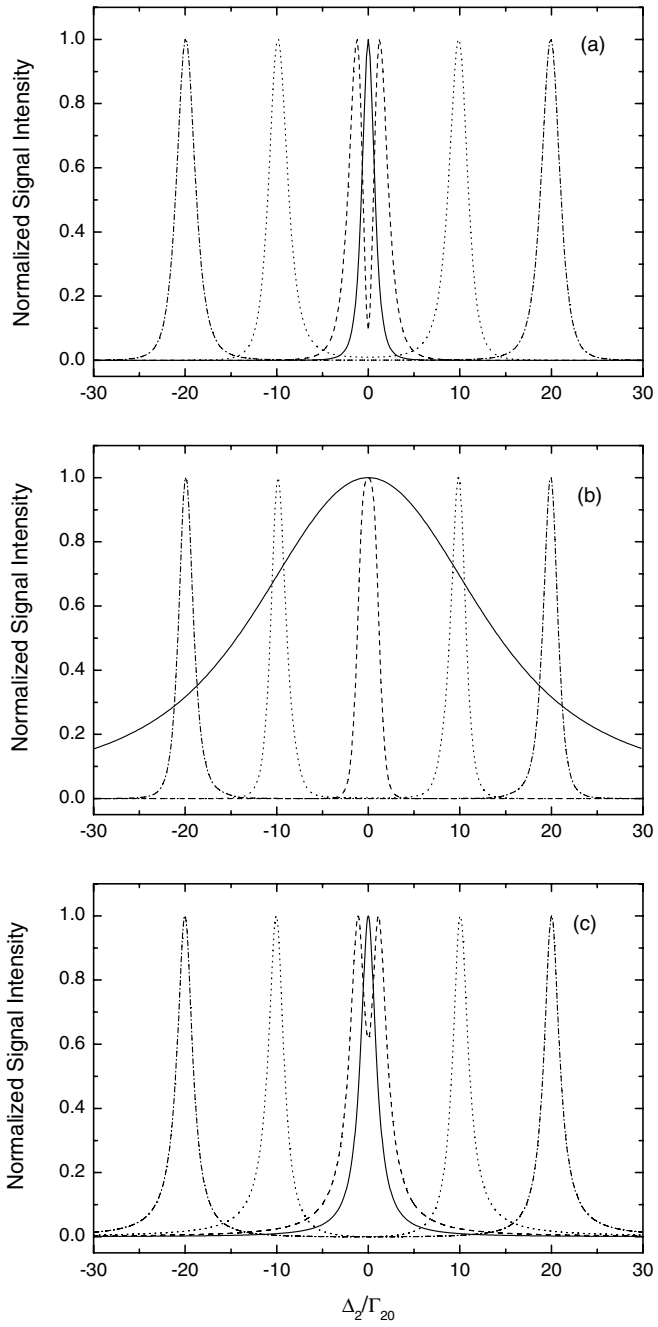

FIG. 11. NFWM spectra in the presence of the coupling field for $G_3/\Gamma_{30}=0$ (solid curve), 1 (dashed curve), 10 (dotted curve), and 20 (dot-dashed curve) when both ω_1 and ω_3 are exactly on resonance (i.e., $\Delta_1/\Gamma_{30}=\Delta_3/\Gamma_{30}=0$). Other parameters are $\Gamma_{10}/k_1u=\Gamma_{20}/k_1u=\Gamma_{30}/k_1u=0.02$, $\zeta_3=1.2$, and ζ_2 equal to (a) 1.2 and (b) 0.8. For comparison, (c) presents the corresponding results of the homogeneously broadened cases.

V. DISCUSSION AND CONCLUSION

Quantum interference has led to the observation of many new effects in resonant nonlinear physics. In the conventional EIT-based FWM (Fig. 1), the common feature is that the coupling field is one of the incident beams involved in the FWM process. By contrast, in the dressed-atom two-photon resonant NFWM [Fig. 2(b)], the coupling field is

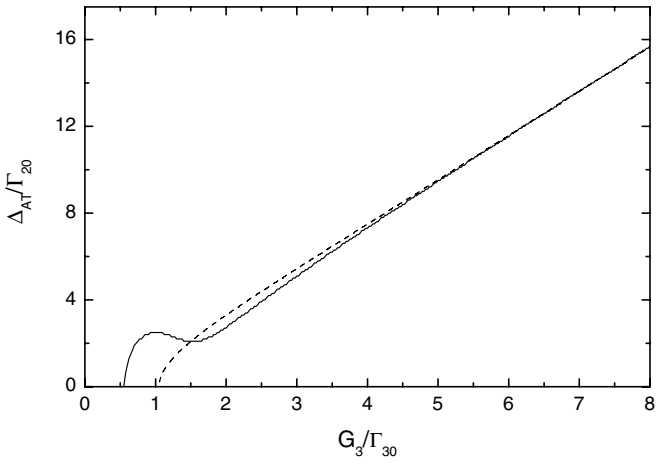

FIG. 12. AT splitting Δ_{AT} versus coupling coefficient G_3 for $\zeta_2=1.2$ (solid curve) and 0.8 (dashed curve) with all the other parameters the same as those used in Fig. 10.

applied to a transition which is not involved in the original NFWM process. Let us now consider the effects of Doppler broadening in these two cases. In the former, the consequence of including Doppler broadening is that the strong coupling fields must be intense enough to induce Rabi frequencies that exceed the Doppler widths before any coherence effects become apparent. By contrast, in the latter the effects of Doppler broadening are more profound. Specifically, we find that if the Doppler broadening is included, then the induced polarization responsible for the NFWM signal becomes sensitive to the atomic velocity. As a result, there exists interference between macroscopic polarizations of atoms with different velocities. This polarization interference can cause significant modification of the NFWM spectra. For example, although the coupling field can suppress the NFWM signal when it is exactly on resonance for the homogeneously broadened case, in the Doppler-broadened system the signal can actually be enhanced when $\zeta_2<1$.

We have also shown that the linewidth of the NFWM spectrum can be reduced significantly by applying a weak coupling field. Previously, it was demonstrated that quantum interference can lead to the cancellation of spontaneous emission. For example, spontaneous emission from a pair of upper levels to a lower level can be reduced or even canceled under certain conditions if the pair is coupled to a fourth level by a coherent driving field [10]. The reduction of the NFWM linewidth reported here is different in physical origin, as the destructive interference between polarizations of atoms with different velocities causes a broadening of the NFWM linewidth. The additional coupling field then controls the degree of the destructive interference, thus reducing the linewidth.

Two-photon resonant NFWM in dressed atoms provides an effective tool for spectroscopic analysis. Let us first consider the case of tuning ω_3 while fixing the frequencies of beams 1 and 2 to the resonances (i.e., $\Delta_1=\Delta_2=0$). In the weak-coupling-field limit $|G_3|^2 \ll \Gamma_{20}\Gamma_{30}$, we have from Eq. (11)

$$I(\omega_3) \propto 1 - 2\left(\frac{\Gamma_{30}}{\Gamma_{20}}\right)\frac{|G_3|^2}{(\omega_3-\Omega_3)^2+\Gamma_{30}^2}, \tag{12}$$

for a homogeneously broadened system. Thus, the resonant frequency Ω_3 and the dephasing rate Γ_{30} can be obtained directly from the ω_3 dependence of the NFWM signal. For example, the dephasing rate between the ground state $6s^2$ and the doubly excited autoionizing Rydberg state $6pnd$ in Ba has been measured by this method [21]. Our technique is also Doppler free in a Doppler-broadened system. As shown in Figs. 7(a) and 7(b), when we scan ω_3 a resonant dip and peak with linewidth $2\Gamma_{30}$ appear for $\zeta_2>1$ and $\zeta_2<1$, respectively. Since the dressed-atom two-photon resonant NFWM involves three-photon resonant excitation in a cascade four-level system, highly excited atomic states can be studied with high sensitivity. Previously, these types of experiments were usually performed in atomic beams, where highly excited atomic states were first excited through multiphoton excitation and then after ionization the resulting electrons or ions were detected. Some time ago an all-optical triple-resonance spectroscopy experiment was performed by Lyyra *et al.* [31], who used lasers to induce state-selective population transfer which was then monitored by detecting the fluorescence. By contrast, dressed-atom two-photon resonant NFWM is a form of coherent spectroscopy, which can be performed in vapor cells, and the signal is a highly directional beam of coherent light. Most importantly, compared with previous methods which usually probe the population of the state $|3\rangle$, our method involves the atomic coherence ρ_{30}; hence, the dephasing rate Γ_{30} between states $|3\rangle$ and $|0\rangle$ can be measured.

Let us now consider the case when ω_2 is scanned in the presence of a strong coupling field of frequency ω_3. In this case the NFWM spectra exhibit Doppler-free AT splitting; thus, two-photon resonant NFWM in dressed atoms can be employed as a new type of high-resolution AT spectroscopy. One important application of the AT effect is to measure the dipole moment because the splitting equals the Rabi frequency of the transition. Currently, most of the AT spectroscopic techniques use three-level systems, where a strong coupling field is tuned to resonance between two states of the system, the induced AT doublet being then probed by a transition to a third level through detection of the probe absorption, induced fluorescence, or photon ionization. The AT spectroscopy proposed here is different from previous types in that two-photon resonant NFWM is employed for probing the energy splitting. There are several advantages to our method. First, where conventionally the splitting is probed by a one-photon transition, here a two-photon process is employed for detecting the AT doublet; thus, transition dipole moments between two highly excited atomic states [$|2\rangle$ and $|3\rangle$ in Fig. 2(b)] can be measured. These states can have very long radiative lifetimes so that direct detection of the fluorescence is difficult. This is because $|2\rangle$ is driven back to the intermediate state $|1\rangle$ by beam $2'$ and coherent radiation is emitted when $|1\rangle-|0\rangle$ is a strongly coupled transition. In addition, two-photon resonant NFWM is a type of high-resolution laser spectroscopy; hence, AT splitting that is much smaller than the Doppler linewidth can be observed.

In this paper we have distinguished between an interference that is internal to the atom and a macroscopic effect that we term polarization interference. On the other hand, other macroscopic effects such as the effects of propagation and phase matching have been ignored. These effects can be investigated by solving Maxwell's equations. As is well known, in the conventional EIT-based FWM, a strong coupling field induces transparency for the FWM signal. By contrast, in the dressed-atom two-photon resonant NFWM the coupling field does not directly create an EIT window at the frequency ω_1 of the NFWM signal. Using the slowly varying envelope approximation, Maxwell's equation for the complex field ε_s of the NFWM signal, which propagates along the $-\mathbf{z}$ direction, becomes

$$\frac{d\varepsilon_s}{dz} = \frac{\alpha_1}{2}\varepsilon_s - i\frac{2\pi\omega_1}{n_1 c}P_T \exp(i\Delta k z), \tag{13}$$

where $\Delta k = k_1 - k_p$ and α_1 and n_1 are the absorption coefficient and refractive index at the frequency ω_1, respectively. In NFWM, the coherence length is given by $l_c = 2c/[n_1(\omega_2/\omega_1)|\omega_2 - \omega_1|\theta^2]$ [32], with θ being the angle between beams 2 and 2′. For a typical experiment, θ is small so that l_c is larger than the interaction length L, as has been demonstrated in Refs. [21,32]. Thus the phase mismatch can be neglected and we have $\Delta k \simeq 0$. Moreover, the amplitudes of the incident fields of frequencies ω_2 and ω_3 (i.e., beams 2, 2′, and 3) can be treated as constant, while due to the absorption the amplitude of the field of beam 1, which has frequency ω_1, varies as $\varepsilon_1(z) = \varepsilon_1(L)\exp[-\alpha_1(L-z)/2]$, leading to $P_T(z) = P_T(L)\exp[-\alpha_1(L-z)/2]$. Here the input plane for beam 1 is at $z=L$. With these assumptions, we have the signal at the output plane $z=0$:

$$|\varepsilon_s(0)|^2 = \left(\frac{2\pi\omega_1 L}{n_1 c}\right)^2 |P_T(L)|^2 \exp(-\alpha_1 L). \tag{14}$$

In the dressed-atom two-photon resonant NFWM we are interested in the ω_2 or ω_3 dependence of the NFWM signal intensity, with ω_1 fixed. Since no EIT window is created at the frequency ω_1, n_1 and α_1 are not dependent on ω_2 and ω_3, so as a result the effects of propagation and phase matching will not affect the overall interference picture discussed in this paper.

In conclusion, we have studied dressed-atom two-photon resonant NFWM in a Doppler-broadened system. It is found that there exists interference between macroscopic polarizations from different ensembles of atoms within the atomic velocity distribution. This polarization interference can cause significant modification of the NFWM spectra. We have also shown that two-photon resonant NFWM in dressed atoms can be employed as a Doppler-free high-resolution AT spectroscopy for measuring transition dipole moments between two highly excited atomic states.

ACKNOWLEDGMENTS

The authors gratefully acknowledge financial support from the National Natural Science Foundation of China under Grants Nos. 10374113, 10574155, and 60578029 and from the National Program for Basic Research in China Grant No. 2001CB309301.

[1] S. E. Harris, Phys. Today **50**(7), 36 (1997).
[2] K. J. Boller, A. Imamoglu, and S. E. Harris, Phys. Rev. Lett. **66**, 2593 (1991).
[3] M. O. Scully, Phys. Rev. Lett. **67**, 1855 (1991).
[4] S. E. Harris, J. E. Field, and A. Imamoglu, Phys. Rev. Lett. **64**, 1107 (1990).
[5] G. Z. Zhang, K. Hakuta, and B. P. Stoicheff, Phys. Rev. Lett. **71**, 3099 (1993).
[6] J. C. Petch, C. H. Keitel, P. L. Knight, and J. P. Marangos, Phys. Rev. A **53**, 543 (1996).
[7] C. H. Keitel, Phys. Rev. A **57**, 1412 (1998).
[8] A. S. Zibrov, M. D. Lukin, and M. O. Scully, Phys. Rev. Lett. **83**, 4049 (1999).
[9] M. Jain, H. Xia, G. Y. Yin, A. J. Merriam, and S. E. Harris, Phys. Rev. Lett. **77**, 4326 (1996).
[10] S. Y. Zhu and M. O. Scully, Phys. Rev. Lett. **76**, 388 (1996); H. R. Xia, C. Y. Ye, and S. Y. Zhu, *ibid.* **77**, 1032 (1996).
[11] M. Koch, J. Feldmann, G. von Plessen, E. O. Göbel, P. Thomas, and K. Köhler, Phys. Rev. Lett. **69**, 3631 (1992).
[12] J. E. Rothenberg and D. Grischkowsky, Opt. Lett. **10**, 22 (1985).
[13] D. DeBeer, L. G. Van Wagenen, R. Beach, and S. R. Hartmann, Phys. Rev. Lett. **56**, 1128 (1986).
[14] P. Fu, Z. Yu, X. Mi, X. Li, and Q. Jiang, Phys. Rev. A **50**, 698 (1994).
[15] P. Fu, X. Mi, Z. Yu, Q. Jiang, Y. Zhang, and X. Li, Phys. Rev. A **52**, 4867 (1995).
[16] X. Mi, Z. Yu, Q. Jiang, X. Li, and P. Fu, Opt. Commun. **152**, 361 (1998).
[17] P. Fu, Y. Wang, Q. Jiang, X. Mi, and Z. Yu, J. Opt. Soc. Am. B **18**, 370 (2001).
[18] H. Ma and C. B. de Araújo, Phys. Rev. Lett. **71**, 3649 (1993).
[19] H. Ma, L. H. Acioli, A. S. L. Gomes, and C. B. de Araújo, Opt. Lett. **16**, 630 (1991).
[20] H. Ma, A. S. L. Gomes, and C. B. de Araújo, Opt. Lett. **17**, 1052 (1992).
[21] J. Sun, Z. Zuo, X. Mi, Z. Yu, Q. Jiang, Y. Wang, L.-A. Wu, and P. Fu, Phys. Rev. A **70**, 053820 (2004).
[22] S. P. Tewari and G. S. Agarwal, Phys. Rev. Lett. **56**, 1811 (1986).
[23] S. H. Autler and C. H. Townes, Phys. Rev. **100**, 703 (1955).
[24] P. B. Hogan, S. J. Smith, A. T. Georges, and P. Lambropoulos, Phys. Rev. Lett. **41**, 229 (1978).
[25] J. Qi, F. C. Spano, T. Kirova, A. Lazoudis, J. Magnes, L. Li, L. M. Narducci, R. W. Field, and A. M. Lyyra, Phys. Rev. Lett. **88**, 173003 (2002).
[26] P. W. Fox, S. I. Gilbert, L. Hollberg, J. H. Marquardt, and H. G. Robinson, Opt. Lett. **18**, 1456 (1993).

[27] J. von Zanthier, C. Skornia, G. S. Agarwal, and H. Walther, Phys. Rev. A **63**, 013816 (2000).

[28] R. Shimano and M. Kuwata-Gonokami, Phys. Rev. Lett. **72**, 530 (1994).

[29] Y. S. Bai, T. W. Mossberg, N. Lu, and P. R. Berman, Phys. Rev. Lett. **57**, 1692 (1986).

[30] C. Wei, N. B. Manson, and J. P. D. Martin, Phys. Rev. Lett. **74**, 1083 (1995).

[31] A. M. Lyyra, H. Wang, T.-J. Whang, W. C. Stwalley, and L. Li, Phys. Rev. Lett. **66**, 2724 (1991).

[32] P. Fu, Q. Jiang, X. Mi, and Z. Yu, Phys. Rev. Lett. **88**, 113902 (2002).